

Gravitationally induced inhibitions of dispersion according to the Schrödinger-Newton Equation

Domenico Giulini and André Großardt
Center of Applied Space Technology and Microgravity
University of Bremen
Am Fallturm 1
D-28359 Bremen, Germany
and
Institute for Theoretical Physics
Leibniz University Hannover
Appelstrasse 2
D-30167 Hannover, Germany

Abstract

We re-consider the time dependent Schrödinger-Newton equation as a model for the self-gravitational interaction of a quantum system. We numerically locate the onset of gravitationally induced inhibitions of dispersion of Gaussian wave packets and find them to occur at mass values more than 6 orders of magnitude higher than reported by Salzman and Carlip [9, 2], namely at about 10^{10} u. This fits much better to simple analytical estimates but unfortunately also questions the experimental realisability of the proposed laboratory test of quantum gravity in the foreseeable future, not just because of large masses, but also because of the need to provide sufficiently long coherence times.

1 Introduction

In this paper we investigate the time dependent Schrödinger-Newton equation (henceforth abbreviated SN-equation):

$$i\hbar\partial_t\Psi(t,\vec{x}) = \left(-\frac{\hbar^2}{2m}\Delta - Gm^2 \int \frac{|\Psi(t,\vec{y})|^2}{\|\vec{x}-\vec{y}\|} d^3y\right) \Psi(t,\vec{x}). \quad (1)$$

It can be thought of as ordinary time-dependent Schrödinger equation,

$$i\hbar\partial_t\Psi(t,\vec{x}) = \left(-\frac{\hbar^2}{2m}\Delta + m\Phi(t,\vec{x})\right) \Psi(t,\vec{x}), \quad (2)$$

with a Newtonian gravitational potential Φ sourced by a mass distribution associated to Ψ itself, that is $m|\Psi|^2$, so that

$$\Delta\Phi(t,\vec{x}) = 4\pi G m |\Psi(t,\vec{x})|^2. \quad (3)$$

The re-coupling of Ψ via (3) into (2) results in the non-linear and non-local self-interaction seen in (1). Physical intuition suggests this self-interaction to cause a slow down of dispersion which should be the more pronounced the higher the value of m is chosen.

In [9, 2] it was surprisingly found on the basis of numerical computations that Gaussian wave packets of width $a \approx 0.5 \mu\text{m}$ start shrinking in width if the mass parameter exceeds $m \approx 1600 \text{ u}$. This is surprising in view of the fact that simple analytical estimates suggest this type of behaviour to occur much later, namely at the said initial width for mass values between around 10^{10} u . The authors of [9, 2] observed this discrepancy and encouraged a check of their results, which we performed. The result is, that our numerical studies now fully confirm the high mass values so that no discrepancy between numerical and simple analytical estimates seem to occur.

The special attention to typical width dimension of $a \approx 0.5 \mu\text{m}$ stems from actual molecular interferometry experiments in which the wave nature of complex molecules has been demonstrated; see, e. g., [1] for an overview. The molecules used in [4] were tetraphenylporphyrin $C_{44}H_{30}N_4$ with mass 614 u and the more complex and more massive fluorofullerene $C_{60}F_{48}$ composed of 108 atoms and of total mass 1632 u . The grating period and grating thickness were about 991 nm and 500 nm respectively.

For further discussion, we now collect some background material concerning the SN-equation (1).

2 Basic features of the Schrödinger-Newton Equation

Equation (1) can be derived from the following action (we write $\dot{\Psi}$ instead of $\partial_t \Psi$ and Ψ^* for the complex conjugate of Ψ):

$$\begin{aligned} \mathcal{S}[\Psi, \Psi^*] = \int dt \left\{ \frac{i\hbar}{2} \int d^3x \left(\Psi^*(t, \vec{x}) \dot{\Psi}(t, \vec{x}) - \Psi(t, \vec{x}) \dot{\Psi}^*(t, \vec{x}) \right) \right. \\ \left. - \frac{\hbar^2}{2m} \int d^3x (\vec{\nabla} \Psi(t, \vec{x})) \cdot (\vec{\nabla} \Psi^*(t, \vec{x})) \right. \\ \left. + \frac{Gm^2}{2} \iint d^3x d^3y \frac{|\Psi(t, \vec{x})|^2 |\Psi(t, \vec{y})|^2}{\|\vec{x} - \vec{y}\|} \right\}. \end{aligned} \quad (4)$$

Note that Ψ and Ψ^* are to be varied independently. A local form can be obtained if the Newtonian gravitational field Φ is introduced:

$$\begin{aligned} \mathcal{S}[\Psi, \Psi^*, \Phi] = \int dt \int d^3x \left\{ \frac{i\hbar}{2} \left(\Psi^*(t, \vec{x}) \dot{\Psi}(t, \vec{x}) - \Psi(t, \vec{x}) \dot{\Psi}^*(t, \vec{x}) \right) \right. \\ \left. - \frac{\hbar^2}{2m} (\vec{\nabla} \Psi(t, \vec{x})) \cdot (\vec{\nabla} \Psi^*(t, \vec{x})) \right. \\ \left. - \frac{1}{8\pi G} (\vec{\nabla} \Phi(t, \vec{x})) \cdot (\vec{\nabla} \Phi(t, \vec{x})) \right. \\ \left. - m |\Psi(t, \vec{x})|^2 \Phi(t, \vec{x}) \right\}. \end{aligned} \quad (5)$$

Variation of (5) with respect to Φ gives (3). Inserting the solution $\Phi = 4\pi Gm\Delta^{-1}|\Psi|^2$ into (5) then leads to (4).

We usually restrict attention to solutions which are square integrable over space, so that solutions of the time dependent SN-equations are paths in the Hilbert space $L^2(\mathbb{R}^3, d^3x)$. We shall see below that time evolution preserves the norm (this follows from the symmetry under phase transformations).

Symmetries of (1) are:

1. Constant phase shifts

$$\Psi \mapsto \Psi', \quad \Psi'(t, \vec{x}) := \exp(i\alpha)\Psi(t, \vec{x}) \quad (6)$$

with constant $\alpha \in \mathbb{R}$. This symmetry of the equation of motion is also a symmetry of the action (4). Hence there is a conserved Noether current which turns out to be just the same functional of Ψ as in ordinary Schrödinger theory. In particular, the space integral over $|\Psi|^2$ is time independent.

2. Proper orthochronous Galilei Transformations

$$(t, \vec{x}) \rightarrow \tau_g(t, \vec{x}) := (t + b, \mathbf{R} \cdot \vec{x} + \vec{v}t + \vec{a}), \quad (7)$$

where $\mathbf{R} \in \text{SO}(3)$ denotes spatial rotations, $\vec{v} \in \mathbb{R}^3$ boost transformations, and $a \in \mathbb{R}^3$ and $b \in \mathbb{R}$ space and time translations respectively, and where g collectively stands for $(\mathbf{R}, \vec{v}, \vec{a}, b)$. These generate the inhomogeneous (proper orthochronous) Galilei group which acts via proper ray-representations on wave functions as follows:

$$\Psi \rightarrow T_g \Psi := \exp(i\beta_g)(\Psi \circ \tau_{g^{-1}}) \quad (8)$$

Note that except for the phase $\exp(i\beta_g)$, this is just the transformation of a scalar function on spacetime under the diffeomorphism τ_g . The g -dependent phase function $\beta : \mathbb{R}^4 \rightarrow \mathbb{R}$ is determined up to spacetime independent additions. A convenient choice is (compare [3])

$$\beta_g(t, \vec{x}) = \frac{m}{\hbar} \left[\vec{v} \cdot (\vec{x} - \vec{a}) - \frac{1}{2} \vec{v}^2 (t - b) \right]. \quad (9)$$

It is immediate that the self-interaction term in (1) and (4) does not affect Galilei invariance of the equation of motion. Moreover, (8) is also a symmetry of the action so that 10 conserved quantities result. The expressions for total momentum and angular momentum are again the same functionals of Ψ as in ordinary Schrödinger theory, but that for total energy will clearly include the non-linear interaction.

3. Whereas the proper orthochronous Galilei transformations exclude space and time inversions, the latter are also symmetries of the SN-equation. To define them, let π and τ be the following diffeomorphisms of \mathbb{R}^4 :

$$\pi : \mathbb{R}^4 \rightarrow \mathbb{R}^4, \quad (t, \vec{x}) \mapsto (t, -\vec{x}), \quad (10a)$$

$$\tau : \mathbb{R}^4 \rightarrow \mathbb{R}^4, \quad (t, \vec{x}) \mapsto (-t, \vec{x}). \quad (10b)$$

The unitary transformations of space inversion and the anti-unitary transformation of time inversion (or better “reversal of motion”) on wavefunctions is then defined by

$$P\Psi := \Psi \circ \pi^{-1}, \quad (11a)$$

$$T\Psi := C \circ \Psi \circ \tau^{-1}, \quad (11b)$$

where C denotes complex-conjugation. It is easy to check that if Ψ solves the SN-equation then $P\Psi$ and $T\Psi$ also solve it.

4. There is a scaling equivariance between SN-equations of different mass parameters m . The precise statement is this: Let \mathbb{R}_+ be the multiplicative group of positive real numbers. It acts by scaling transformations on spacetime:

$$\sigma : \mathbb{R}_+ \times \mathbb{R}^4 \rightarrow \mathbb{R}^4, \quad \sigma(\mu, (t, \vec{x})) = \sigma_\mu(t, \vec{x}) = (\mu^a t, \mu^b \vec{x}), \quad (12)$$

where a, b are real numbers characterising the action. It also acts on the complex numbers:

$$s : \mathbb{R}_+ \times \mathbb{C} \rightarrow \mathbb{C}, \quad s(\mu, z) = s_\mu(z) = \mu^c z, \quad (13)$$

where c is yet another real number. Now, since the group acts on \mathbb{R}^4 (via σ) and \mathbb{C} (via s) it also acts on $\mathbb{R}^4 \times \mathbb{C}$ (via $\sigma \times s$) and hence on graphs of functions $\Psi : \mathbb{R}^4 \rightarrow \mathbb{C}$. The transform of a function (via S) is then defined to be the function uniquely corresponding to the transformed graph:

$$\begin{aligned} \text{graph}(S_\mu \Psi) &:= \sigma_\mu \times s_\mu(\text{graph}(\Psi)) \\ &= \bigcup_{(t, \vec{x}) \in \mathbb{R}^4} \left(\sigma_\mu(t, \vec{x}), s_\mu(\Psi(t, \vec{x})) \right) \\ &= \bigcup_{(t, \vec{x}) \in \mathbb{R}^4} \left((t, \vec{x}), s_\mu \circ \Psi \circ \sigma_\mu^{-1}(t, \vec{x}) \right), \end{aligned} \quad (14)$$

where in the last step we just used that each σ_μ is a bijection. Hence

$$\begin{aligned} S : \mathbb{R}_+ \times \text{Funct}(\mathbb{R}^4, \mathbb{C}) &\rightarrow \text{Funct}(\mathbb{R}^4, \mathbb{C}), \\ S(\mu, \Psi) &= S_\mu(\Psi) = s_\mu \circ \Psi \circ \sigma_\mu^{-1}. \end{aligned} \quad (15)$$

or, in simpler terms,

$$S_\mu \Psi(t, \vec{x}) = \mu^c \Psi(\mu^{-a} t, \mu^{-b} \vec{x}). \quad (16)$$

As already mentioned, we wish to consider normalised wave functions. The scaling (15) preserves normalisation iff $2b + 3c = 0$, i.e. iff $c = -3b/2$. Solutions to the SN-equation for all positive mass parameters m then correspond to special paths on the unit sphere in Hilbert space. We ask under what conditions the action (15) transforms solutions Ψ to the SN-equation for mass parameter m to solutions $S_\mu \Psi$ for some mass parameter m_μ . We have

$$\partial_t S_\mu \Psi = \mu^{-a} S_\mu \partial_t \Psi \quad (17a)$$

$$m_\mu^{-1} \Delta S_\mu \Psi = \mu^{-2b} (m/m_\mu) m^{-1} S_\mu \Delta \Psi \quad (17b)$$

$$m_\mu^2 U(S_\mu \Psi) S_\mu \Psi = (m_\mu/m)^2 \mu^{-b} m^2 S_\mu (U(\Psi) \Psi), \quad (17c)$$

where $U(\Psi)$ is the potential function

$$U(\Psi)(t, \vec{x}) = \int \frac{|\Psi(t, \vec{y})|^2}{\|\vec{x} - \vec{y}\|} d^3x. \quad (18)$$

Denoting the SN-equation symbolically by $SN(m, \Psi) = 0$, we have

$$SN(m, \Psi) = 0 \Rightarrow SN(m_\mu, S_\mu \Psi) = 0 \quad (19)$$

iff each term scales with the same factor. According to (17) this is the case iff

$$\mu^{-a} = \mu^{-2b} (m/m_\mu) = \mu^{-b} (m_\mu/m)^2 \quad (20)$$

i. e. iff

$$\frac{m_\mu}{m} = \mu^{-b/3} = \mu^{-a/5}. \quad (21)$$

First of all this means that m_μ is a power of μ times m . This power may without loss of generality be taken to unity, for if m_μ/m were equal to μ^d we could take $\mu' := \mu^d$ as new and equally good scaling parameter and everything that follows were true for μ' instead of μ . So from $m_\mu/m = \mu$ we see from (21) that $b = -3$, $a = -5$, and hence $c = 9/2$. To sum up, we have shown that

$$S_\mu \Psi(t, \vec{x}) = \mu^{9/2} \Psi(\mu^5 t, \mu^3 \vec{x}) \quad (22)$$

satisfies the SN-equation for mass $m_\mu = \mu \cdot m$ if Ψ satisfies the SN-equation for mass m .¹

The stationary version of (1) is obtained by replacing $i\hbar\partial_t$ with the energy E . It has a unique (up to translations, of course) spherically symmetric stable ground state. The ground state minimises the energy functional which is given by the negative of the second and third term in (4). Existence and uniqueness of the ground state were first shown by Lieb [6], albeit motivated in completely different physical context (one-component plasmas) in 1976 by Choquard. Hence Lieb called it the *Choquard equation*, which is mathematically equivalent to the stationary SN-equation.

Numerical studies led to the following value for the ground-state energy²

$$E_0 = -0.163 \frac{G^2 m^5}{\hbar^2} = -0.163 \cdot mc^2 \cdot \left(\frac{m}{m_P}\right)^4, \quad (23)$$

where

$$m_P := \sqrt{\frac{\hbar c}{G}} = 1.221 \times 10^{19} \text{ GeV}/c^2 = 21.76 \mu\text{g} \quad (24)$$

is the Planck mass. A rough intuition for the width, a , of the mass distribution $m|\Psi|^2$ in the ground state is obtained by schematically writing the total energy as sum of

¹ Formulae (2.3) of [9] and (2.4) of [2] seem to be incorrect.

² See [8] for an early attempt and [5] for a more recent and far more detailed account, also showing linear stability of the lowest and linear instability of all higher spherically symmetric stationary states found earlier in [7]. The 20 lowest energies are tabulated in Table 1 of [5] and range from -0.163 to -0.000221 times $G^2 m^5 / \hbar^2$.

the kinetic and potential term and replacing the Laplacian in the first by a^{-2} and the double integral in the third term of (4) by a^{-1} :

$$E \approx \frac{\hbar^2}{2ma^2} - \frac{Gm^2}{2a}. \quad (25)$$

Minimising in a then gives

$$a_0 \approx \frac{2\hbar^2}{Gm^3} = 2\ell_P \cdot \left(\frac{m_p}{m}\right)^3, \quad (26)$$

where

$$\ell_P := \sqrt{\frac{\hbar G}{c^3}} = 1.616 \times 10^{-35} \text{ m} \quad (27)$$

is the Planck length. The rough energy (25) at the rough minimum (26) is

$$E_0 \approx -\frac{1}{8} \cdot \frac{G^2 m^5}{\hbar^2} \quad (28)$$

which compares reasonably with (23).

Clearly, we would not trust the stationary solution in this Newtonian picture if the support of the mass distribution $m|\Psi|^2$ had a spatial extent not much larger than m 's Schwarzschild radius Gm/c^2 . Now, the condition $a_0 \gg Gm/c^2$ is equivalent to

$$m^4 \ll 2 \cdot m_P^4, \quad (29)$$

which means that we should not let m come too close to the Planck mass (though note the 4th powers).

Finally we note the dimensionless form of (1) that one obtains by introducing a spatial length scale ℓ . Using dimensionless spatial coordinates \vec{x}' and a dimensionless time t' according to

$$\vec{x}' := \vec{x}/\ell, \quad t' := t \cdot \frac{\hbar}{2m\ell} \quad (30)$$

and rescaling $\Psi \mapsto \Psi' := \ell^{3/2} \cdot \Psi$ so as to keep Ψ' normalised with respect to d^3x' , we get

$$i\partial_{t'}\Psi'(t', \vec{x}') = \left(-\Delta' - K \int \frac{|\Psi'(t', \vec{y}')|^2}{\|\vec{x}' - \vec{y}'\|} d^3y' \right) \Psi'(t', \vec{x}') \quad (31)$$

with dimensionless coupling constant

$$K = 2 \cdot \frac{Gm^3\ell}{\hbar^2} = 2 \cdot \left(\frac{\ell}{\ell_P}\right) \left(\frac{m}{m_P}\right)^3. \quad (32)$$

Note that the combination (length) \times (mass)³ which determines the coupling had to be expected from scale invariance (22).

3 Analytical Estimations of the Collapse Mass

We consider now the time-dependent SN-equation for initial values given by a spherically symmetric Gaussian wave packet of width a :

$$\Psi(r, t = 0) = (\pi a^2)^{-3/4} \exp\left(-\frac{r^2}{2a^2}\right). \quad (33)$$

We have then two free parameters, a and m , and we ask for the regions in this two-parameters space in which significant inhibitions of the usual free dispersion occur. For simplicity we will refer to such a behaviour as a “collapse”, even though it is clear that neither the integral over $|\psi|^2$ nor the volume of the support of $|\psi|^2$ (which is infinite) change. We start by presenting four different analytical arguments, all of which suggest that a collapse of the wave packet sets in whenever the dimensionless coupling K in (32) approaches unity.

3.1 Equilibrium of Forces for the Free Solution

Let us first give a rough estimate for the critical mass by a naïve calculation, in which we demand equilibrium between the acceleration of the peak probability density and the acceleration due to gravitation for a point mass.

The free solution (without gravitational potential) for the problem at hand is

$$\Psi_{\text{free}}(r, t) = (\pi a^2)^{-3/4} \left(1 + \frac{i \hbar t}{m a^2}\right)^{-3/2} \exp\left(-\frac{r^2}{2a^2 \left(1 + \frac{i \hbar t}{m a^2}\right)}\right). \quad (34)$$

The radial probability density, $\rho(r, t) = 4\pi r^2 |\Psi_{\text{free}}(r, t)|^2$, has a global maximum at

$$r_p = a \sqrt{1 + \frac{\hbar^2 t^2}{m^2 a^4}}. \quad (35)$$

Taking the second time derivative we obtain the peak’s acceleration

$$\ddot{r}_p = \frac{\hbar^2}{m^2 a^3} \left(1 + \frac{\hbar^2 t^2}{m^2 a^4}\right)^{-3/2} = \frac{\hbar^2}{m^2 r_p^3}. \quad (36)$$

This we now compare to Newton’s law for the gravitational acceleration

$$\ddot{r} = \frac{G m}{r^2}, \quad (37)$$

at time $t = 0$. Using $r_p(t = 0) = a$, we get

$$m = \left(\frac{\hbar^2}{G a}\right)^{1/3}. \quad (38)$$

For $a = 0.5 \mu\text{m}$ this yields a threshold mass for collapse of about $7 \times 10^{-18} \text{ kg}$ or $4 \times 10^9 \text{ u}$.

3.2 Lower Mass Bound for Negative Energy Solutions

It was noted by Harrison *et al.* [5] that only initial data of negative energy can show inhibitions of dispersion. This can be used to provide a lower mass bound for collapsing behaviour in a mathematically rigorous way. The result strongly contradicts the collapse mass found in [9, 2].

Define the kinetic energy T , the potential energy V , and the total energy \mathcal{E} respectively by

$$\begin{aligned}\mathcal{E} &= T + \frac{1}{2} V = \frac{\hbar^2}{2m} \int d^3x |\nabla \Psi(\vec{x})|^2 + \frac{m}{2} \int d^3x \Phi |\Psi(\vec{x})|^2 \\ &= \frac{\hbar^2}{2m} \int d^3x |\nabla \Psi(\vec{x})|^2 - \frac{Gm^2}{2} \int d^3x \int d^3y \frac{|\Psi(\vec{x})|^2 |\Psi(\vec{y})|^2}{|\vec{x} - \vec{y}|}.\end{aligned}\quad (39a)$$

The second moment, defined by

$$Q = \int |\vec{x}|^2 |\Psi|^2 d^3x, \quad (40)$$

then has the following second order time derivative:

$$\ddot{Q} = \frac{2\hbar^2}{m^2} \int |\nabla \Psi|^2 d^3x + \int \Phi |\Psi|^2 d^3x = \frac{1}{m} (4T + V) = \frac{1}{m} (4\mathcal{E} - V). \quad (41)$$

But Φ (and therefore also V) is everywhere negative due to the maximum principle which means that for positive energy \mathcal{E} , Q is a convex function of time. Hence, in terms of the second moment it is a necessary (but not sufficient) condition for a collapsing wave packet, that its initial data has negative energy.

We can now easily calculate the energy of the spherically symmetric, real Gaussian wave packet (33). It is

$$\begin{aligned}\mathcal{E} &= \frac{2\pi \hbar^2}{m} \int_0^\infty dr (\partial_r \Psi(r))^2 - 8\pi^2 G m^2 \\ &\quad \times \int_0^\infty dr \left[\int_0^r dr' \frac{r'^2}{r} \Psi^2(r) \Psi^2(r') + \int_r^\infty dr' r' \Psi^2(r) \Psi^2(r') \right] \\ &= \frac{2\hbar^2}{\sqrt{\pi} m a^7} \int_0^\infty dr r^2 e^{-r^2/a^2} - \frac{8Gm^2}{\pi a^6} \int_0^\infty dr \frac{e^{-r^2/a^2}}{r} \\ &\quad \times \left[\int_0^r dr' r'^2 e^{-r'^2/a^2} + r \int_r^\infty dr' r' e^{-r'^2/a^2} \right] \\ &= \frac{\hbar^2}{2ma^4} - \frac{2Gm^2}{\sqrt{\pi} a^3} \sinh^{-1}(1).\end{aligned}\quad (42)$$

Now $\mathcal{E} < 0$ is equivalent to

$$m > \left(\frac{\sqrt{\pi} \hbar^2}{4 G a \sinh^{-1}(1)} \right)^{1/3} \approx \left(\frac{\hbar^2}{2 G a} \right)^{1/3} \quad (43)$$

By inserting $a = 0.5 \mu\text{m}$ again this yields the lower mass bound for negative energy solutions $m > 5.5 \times 10^{-18} \text{ kg} \approx 3.3 \times 10^9 \text{ u}$.

3.3 Mass of the Stationary Ground State

In our third example we consider the ground state of the spherically symmetric SN-equation found by Moroz *et al.* in [7]. In order to do this we need to rescale the SN-equation in a suitable fashion in order to compare our form of the equation, which explicitly contains the mass parameter, with the form solved in [7], in which m does not appear. In order to understand how to transform solutions of one form into solutions of the other, we use scale invariance.

In a first step we substitute $U = \frac{2m}{\hbar^2}(E - m\Phi)$ into the stationary SN-equation

$$E\Psi(\vec{x}) = \left[-\frac{\hbar^2}{2m}\Delta + m\Phi(\vec{x}) \right] \Psi(\vec{x}), \quad (44a)$$

$$\Delta\Phi(\vec{x}) = 4\pi G m |\Psi(\vec{x})|^2. \quad (44b)$$

It then takes the following form:

$$U(\vec{x})\Psi(\vec{x}) = -\Delta\Psi(\vec{x}), \quad (45a)$$

$$\Delta U(\vec{x}) = -\frac{2m^2}{\hbar^2}\Delta\Phi(\vec{x}) = -\frac{8\pi G m^3}{\hbar^2} |\Psi(\vec{x})|^2. \quad (45b)$$

This can be further simplified if written in terms of the rescaled function $\Omega = \alpha\Psi$, where $\alpha := \sqrt{8\pi G m^3}/\hbar$. We get

$$\Delta\Omega(\vec{x}) = -U(\vec{x})\Omega(\vec{x}), \quad (46a)$$

$$\Delta U(\vec{x}) = -|\Omega(\vec{x})|^2. \quad (46b)$$

The norm of Ω is obviously $\|\Omega\| = \alpha \|\Psi\|$.

Now we rescale the mass by a factor of μ , as discussed above. Then, according to equation (22), $S_\mu\Psi(\vec{x}) = \mu^{9/2}\Psi(\mu^3\vec{x})$ and $\alpha \rightarrow \alpha_\mu = \mu^{3/2}\alpha$. Therefore

$$\begin{aligned} S_\mu\Omega(\vec{x}) &= \alpha_\mu S_\mu\Psi(\vec{x}) = \mu^6\alpha\Psi(\mu^3\vec{x}) = \mu^6\Omega(\mu^3\vec{x}), \\ \|S_\mu\Omega\| &= \alpha_\mu \|S_\mu\Psi\| = \mu^{3/2}\alpha \|\Psi\| = \mu^{3/2}\|\Omega\|. \end{aligned} \quad (47)$$

This means that the rescaling changes the norm of Ω and the following statement holds:

Proposition 1. *Suppose that (Ω, U) satisfy (46). For a given mass value m let μ be the rescaling parameter for which the norm of $S_\mu\Omega$ is*

$$\|S_\mu\Omega\| = \frac{\sqrt{8\pi G m^3}}{\hbar}. \quad (48)$$

Then the wave function defined by

$$\Psi(\vec{x}) := \frac{\hbar}{\sqrt{8\pi G m^3}} S_\mu\Omega(\vec{x}) \quad (49)$$

is a normalised solution to the stationary SN-equation (44) with mass parameter m .

Putting equations (47)–(49) together we obtain a formula that gives us a normalised wave function satisfying the stationary SN-equation (45) with mass parameter m for any unnormalised solution Ω of (46):

$$\Psi(\vec{x}) = \frac{(8\pi G)^{3/2} m^{9/2}}{\hbar^3 \|\Omega\|^4} \Omega\left(\frac{8\pi G m^3}{\hbar^2 \|\Omega\|^2} \vec{x}\right). \quad (50)$$

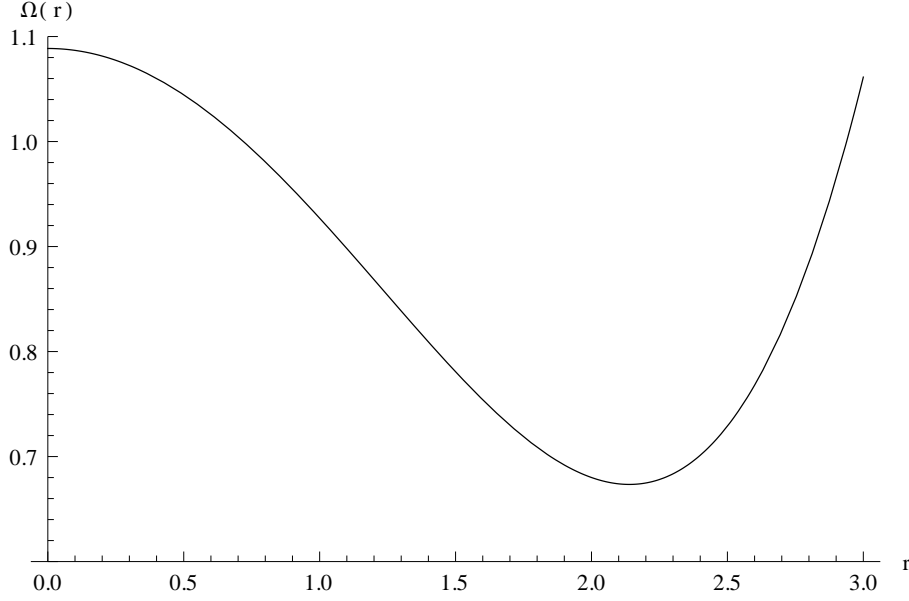


Figure 1: The ground state solution (51) with $\Omega_0 = 1.08864$ found by Moroz *et al.* [7] plotted up to forth order. It seems reasonable from this plot to cut off the solution for values of $r > 2.2$.

In [7] Moroz *et al.* found spherically symmetric, real solutions³

$$\Omega(r) = \Omega_0 \left(1 - \frac{1}{6} r^2 + \frac{\Omega_0^2 + 1}{120} r^4 + \dots \right) \quad (51)$$

to (45), where $\Omega_0 = \Omega(0)$ and $\Omega_0 \approx 1.08864$ for the ground state. These polynomial functions are in general not normalisable but for the right choice of Ω_0 they tend to zero asymptotically as $r \rightarrow \infty$. Nevertheless, for the approximate solution we must introduce a cutoff Λ such that $\Omega(r) \equiv 0$ for $r > \Lambda$. The ground state solution is plotted in figure 1 up to order r^4 , according to which $\Lambda \approx 2.2$ seems to be a reasonable choice. Therefore

$$\|\Omega\|^2 \approx \int_0^\Lambda 4\pi r^2 dr \Omega^2(r) \approx 26. \quad (52)$$

If we define as the width of Ω the cutoff Λ , the width of the wave packet Ψ is

$$a = \frac{\hbar^2 \|\Omega\|^2}{8\pi G m^3} \Lambda \approx \frac{57 \hbar^2}{8\pi G m^3}, \quad (53)$$

or written in terms of m

$$m \approx \left(\frac{57 \hbar^2}{8\pi G a} \right)^{1/3}. \quad (54)$$

With the usual value of $a = 0.5 \mu\text{m}$ we get a mass of

$$m \approx 9.1 \times 10^{-18} \text{ kg} \approx 5.5 \times 10^9 \text{ u}. \quad (55)$$

³ For the spherically symmetric SN-equation, the solution can w.l.o.g. be assumed real. This follows from (45a) if restricted to the spherically symmetric case.

3.4 Short-Time Behaviour

Finally, to obtain the behaviour of the spherically symmetric SN-equation with an initial Gaussian wave packet for small times, we consider the lowest order terms of the series expansion around $t = 0$. Transforming to $\phi(r, t) := r \Psi(r, t)$ and considering the spherically symmetric gravitational potential

$$\Phi(r, t) = -4\pi G m \left[\frac{1}{r} \int_0^r |\phi(r', t)|^2 dr' + \int_r^\infty \frac{|\phi(r', t)|^2}{r'} dr' \right], \quad (56)$$

the SN-equation together with its complex conjugate reads

$$\partial_t \phi = \frac{i\hbar}{2m} \partial_r^2 \phi - \frac{i m}{\hbar} \Phi \phi, \quad \partial_t \phi^* = -\frac{i\hbar}{2m} \partial_r^2 \phi^* + \frac{i m}{\hbar} \Phi \phi^*, \quad (57)$$

where, as before, the star denotes complex conjugation. We get the first order time derivative

$$\partial_t |\phi|^2 = (\partial_t \phi) \phi^* + \phi (\partial_t \phi^*) = \frac{i\hbar}{2m} ((\partial_r^2 \phi) \phi^* - \phi (\partial_r^2 \phi^*)) \quad (58)$$

of the absolute value squared which vanishes at $t = 0$ because $\phi(r, 0)$ is real valued. For the second order time derivatives we obtain

$$\begin{aligned} \partial_t^2 \phi &= \frac{i\hbar}{2m} \partial_r^2 (\partial_t \phi) - \frac{i m}{\hbar} (\partial_t \Phi) \phi - \frac{i m}{\hbar} \Phi (\partial_t \phi) \\ &= -\frac{\hbar^2}{4m^2} \partial_r^4 \phi + \frac{1}{2} (\partial_r^2 \Phi) \phi + (\partial_r \Phi) (\partial_r \phi) + \Phi (\partial_r^2 \phi) \\ &\quad - \frac{m^2}{\hbar^2} \Phi^2 \phi - \frac{i m}{\hbar} (\partial_t \Phi) \phi \end{aligned} \quad (59a)$$

$$\begin{aligned} \partial_t^2 \phi^* &= -\frac{\hbar^2}{4m^2} \partial_r^4 \phi^* + \frac{1}{2} (\partial_r^2 \Phi) \phi^* + (\partial_r \Phi) (\partial_r \phi^*) + \Phi (\partial_r^2 \phi^*) \\ &\quad - \frac{m^2}{\hbar^2} \Phi^2 \phi^* + \frac{i m}{\hbar} (\partial_t \Phi) \phi^* \end{aligned} \quad (59b)$$

$$\begin{aligned} \partial_t^2 |\phi|^2 &= (\partial_t^2 \phi) \phi^* + 2 (\partial_t \phi) (\partial_t \phi^*) + \phi (\partial_t^2 \phi^*) \\ &= -\frac{\hbar^2}{4m^2} [(\partial_r^4 \phi) \phi^* - 2 (\partial_r^2 \phi) (\partial_r^2 \phi^*) + \phi (\partial_r^4 \phi^*)] \\ &\quad + (\partial_r^2 \Phi) |\phi|^2 + (\partial_r \Phi) ((\partial_r \phi) \phi^* + \phi (\partial_r \phi^*)). \end{aligned} \quad (59c)$$

We introduce some shorthand notations

$$\alpha := (\pi a^2)^{-3/2} \quad \beta := a^{-1} \quad \rho := \beta r \quad (60a)$$

$$\gamma_1 := 4\pi^{-1/2} G \alpha \beta \quad \gamma_2 := 2 G \alpha \beta \quad \gamma_3 := \hbar^2 \alpha \beta^2 \quad (60b)$$

$$\tilde{\Phi} := -\alpha \gamma_1^{-1} m^{-1} \Phi \quad \phi_0(r) := \phi(r, 0) = \sqrt{\alpha} r e^{-\beta^2 r^2/2}, \quad (60c)$$

and consider the value of $\partial_t^2 |\phi|^2$ at $t = 0$ which, as $\Phi \sim m$, takes the form

$$\partial_t^2 |\phi|^2|_{t=0} = m A(\rho) + \frac{1}{m^2} B(\rho), \quad (61)$$

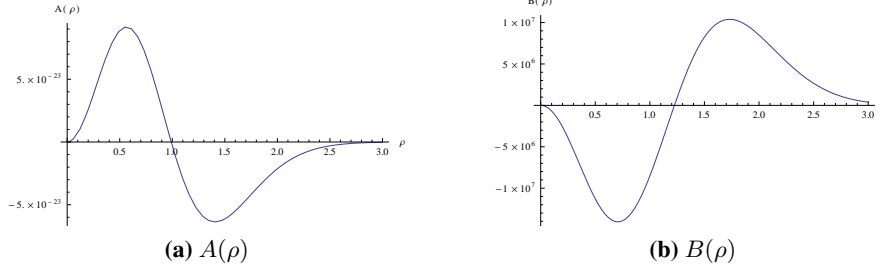


Figure 2: Components $A(\rho)$ and $B(\rho)$ of the order t^2 contribution to $|\phi|^2$ which is proportional to $m A(\rho) + \frac{1}{m^2} B(\rho)$. While A is attractive, B shows a repulsive behaviour.

where

$$A(\rho) = -\frac{\gamma_1}{\alpha} \left((\partial_r^2 \tilde{\Phi}) \phi_0^2 + 2 (\partial_r \tilde{\Phi}) (\partial_r \phi_0) \phi_0 \right) \quad (62)$$

$$B(\rho) = -\frac{\hbar^2}{2} (\phi_0 (\partial_r^4 \phi_0) - (\partial_r^2 \phi_0)^2). \quad (63)$$

Evaluating the derivatives of $\tilde{\Phi}$ we obtain

$$\begin{aligned} \tilde{\Phi} &= \frac{1}{\rho} \int_0^\rho \rho'^2 e^{-\rho'^2} d\rho' + \int_\rho^\infty \rho' e^{-\rho'^2} d\rho' \\ &= \frac{\sqrt{\pi}}{4} \frac{\text{erf}(\rho)}{\rho} \end{aligned} \quad (64a)$$

$$\frac{1}{\beta} \partial_r \tilde{\Phi} = \partial_\rho \tilde{\Phi} = \frac{1}{2\rho} e^{-\rho^2} - \frac{\sqrt{\pi}}{4} \frac{\text{erf}(\rho)}{\rho^2} \quad (64b)$$

$$\frac{1}{\beta^2} \partial_r^2 \tilde{\Phi} = \partial_\rho^2 \tilde{\Phi} = \frac{\sqrt{\pi}}{2} \frac{\text{erf}(\rho)}{\rho^3} - \left(1 + \frac{1}{\rho^2} \right) e^{-\rho^2}, \quad (64c)$$

where $\text{erf}(\rho)$ is the *error function*

$$\text{erf}(\rho) := \frac{2}{\sqrt{\pi}} \int_0^\rho e^{-x^2} dx. \quad (65)$$

Inserting (64b) and (64c) into (62), the final result can now be stated as

$$|\phi|^2 = \phi_0^2 + \frac{t^2}{2} \left(m A(\rho) + \frac{1}{m^2} B(\rho) \right) + \mathcal{O}(t^3), \quad (66)$$

where

$$A(\rho) = 2\gamma_1 \rho^2 e^{-2\rho^2} - \gamma_2 \rho e^{-\rho^2} \text{erf}(\rho) \quad (67)$$

$$B(\rho) = \gamma_3 \rho^2 (2\rho^2 - 3) e^{-\rho^2}. \quad (68)$$

$A(\rho)$ and $B(\rho)$ are plotted in figure 2. While A shows an attractive behaviour (i. e. the wave function grows for small values of ρ), B shows a repulsive behaviour. Thus, the attractive behaviour gets dominant for large masses, as expected.

In figure 3 the second order derivative of $|\phi|^2$ is plotted for several values of the mass m . One can see that there is a repulsive behaviour for $m \lesssim 4 \times 10^9$ u which turns with increasing mass and is completely attractive for masses $m \gtrsim 9 \times 10^9$ u. We therefore expect the collapse of the wave function to happen at about $5\text{--}8 \times 10^9$ u.

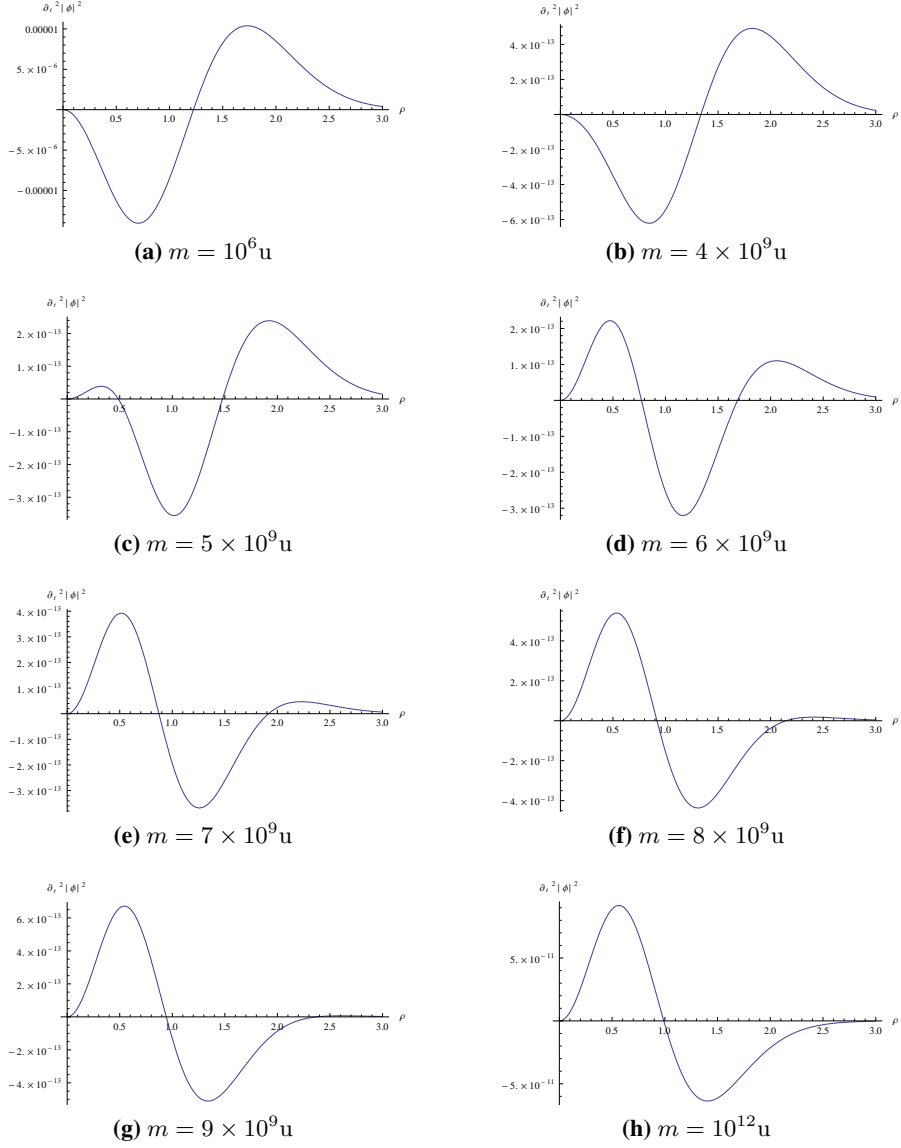


Figure 3: Plot of $\partial_t^2 |\phi|^2$ at $t = 0$ for several masses. While the graph changes only in its quantitative scale and does not change qualitatively in its shape for masses smaller than $m = 4 \times 10^9 \text{u}$ and larger than $m = 9 \times 10^9 \text{u}$, respectively, one can see a qualitative change from repulsive to attractive behaviour in between those mass values.

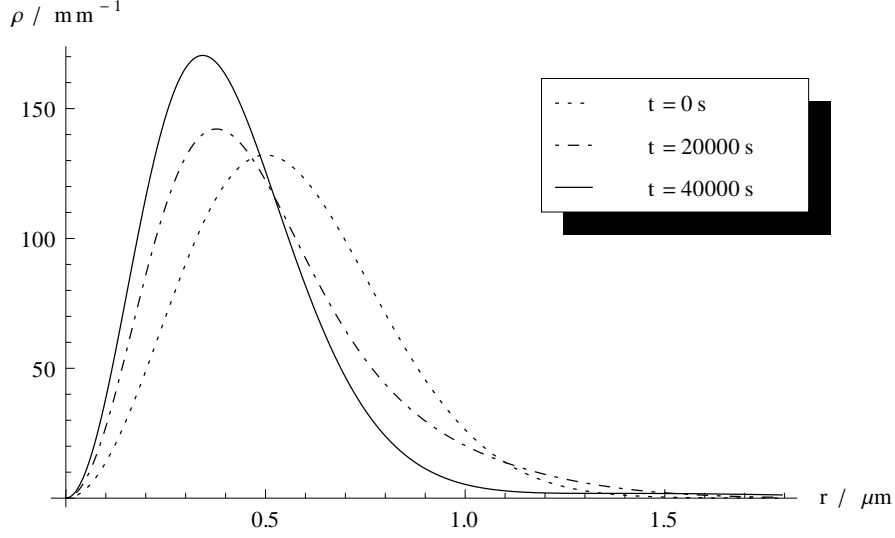


Figure 4: Collapsing wave packet for $m = 7 \times 10^9$ u. Plotted is the radial probability density $\rho = 4\pi r^2 |\psi|^2$ against r at three different times.

4 Numerical Investigation of the time dependent Schrödinger-Newton Equation

Our numerical methods do not differ in principle from those used in [9]. A Crank-Nicolson scheme is applied to solve the differential equation (1) in a spherically symmetric context.

Having defined both a spatial and temporal grid size Δr and Δt and using the index notation $\Psi_j^n = \Psi(j\Delta r, n\Delta t)$ we can write equation (1) in a discretised way using Cayley's form of the SN-equation

$$\exp\left(\frac{i\Delta t}{2\hbar}H\right)\Psi_j^{n+1} = \exp\left(-\frac{i\Delta t}{2\hbar}H\right)\Psi_j^n. \quad (69)$$

Linearising this equation we can write it as

$$\Psi_j^{n+1} = (Q^{-1} - \mathbb{1})\Psi_j^n \quad (70a)$$

$$Q = \frac{1}{2} \left(\mathbb{1} + \frac{i\Delta t}{2\hbar} H \right). \quad (70b)$$

We thus have to solve the linear system

$$Q\chi^n = \Psi^n \quad (71)$$

to obtain

$$\Psi^{n+1} = \chi^n - \Psi^n. \quad (72)$$

The radial component of the Laplacian in spherical coordinates,

$$\Delta_r = \begin{cases} \frac{\partial^2}{\partial r^2} + \frac{2}{r} \frac{\partial}{\partial r} & \text{if } r > 0 \\ 3 \frac{\partial^2}{\partial r^2} & \text{if } r = 0, \end{cases} \quad (73)$$

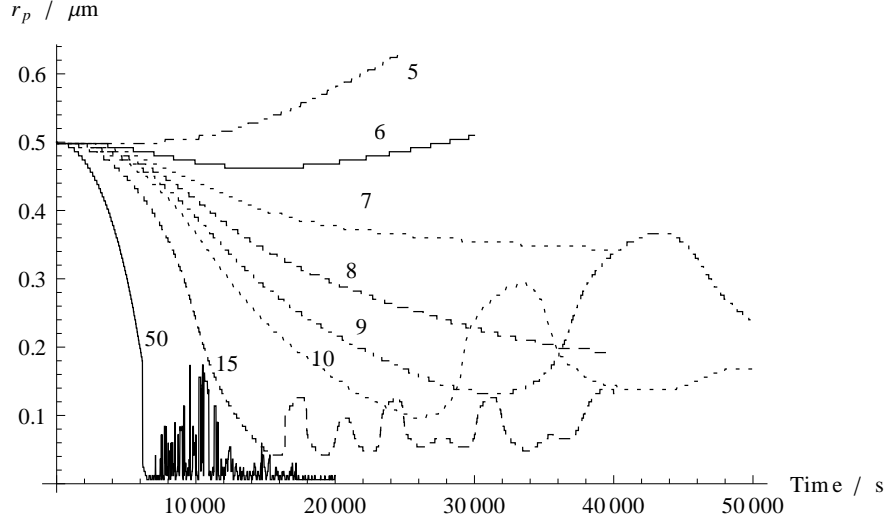


Figure 5: The peak of the radial probability density plotted against time for several masses. The curves are marked with the mass in units of 10^9 u.

takes the discretised form

$$\Delta\chi_j^n = \begin{cases} \frac{1}{(\Delta r)^2} \left(\frac{j-1}{j} \chi_{j-1}^n - 2\chi_j^n + \frac{j+1}{j} \chi_{j+1}^n \right) & \text{if } j > 0 \\ \frac{1}{(\Delta r)^2} (-6\chi_0^n + 6\chi_1^n) & \text{if } j = 0, \end{cases} \quad (74)$$

while the discretised form of the potential

$$\Phi = -4\pi Gm \left(\frac{1}{r} \int_0^r |\Psi(r', t)|^2 r'^2 dr' + \int_r^\infty |\Psi(r', t)|^2 r' dr' \right) \quad (75a)$$

is

$$\Phi_j^n = -4\pi Gm(\Delta r)^2 v_j^n \quad (75b)$$

$$v_j^n = \frac{1}{j} \sum_{i=0}^{j-1} |\Psi_i^n|^2 i^2 + \sum_{i=j}^{N-1} |\Psi_i^n|^2 i. \quad (75c)$$

Q then becomes a tridiagonal matrix

$$Q = \begin{pmatrix} b_0 & c_0 & 0 & 0 & \cdots \\ a_1 & b_1 & c_1 & 0 & \cdots \\ 0 & a_2 & b_2 & c_2 & \\ \vdots & & & \ddots & \vdots \\ 0 & \cdots & a_{N-1} & b_{N-1} \end{pmatrix}, \quad (76)$$

where

$$a_j = \beta \frac{j-1}{j} \quad (0 < j \leq N-1) \quad (77a)$$

$$b_0 = \frac{1}{2} - 6\beta - \gamma v_0 \quad b_j = \frac{1}{2} - 2\beta - \gamma v_j \quad (0 < j \leq N-1) \quad (77b)$$

$$c_0 = 6\beta \quad c_j = \beta \frac{j+1}{j} \quad (0 < j < N-1) \quad (77c)$$

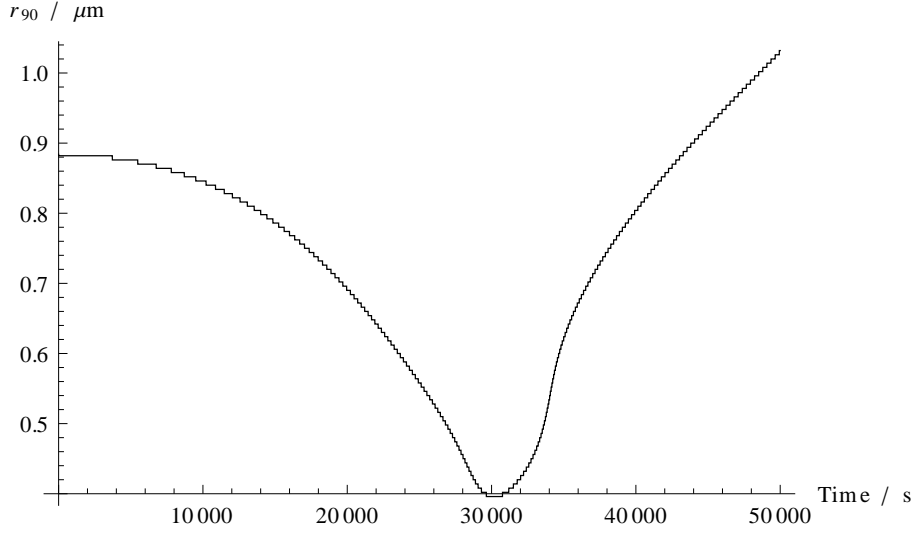


Figure 6: The radius r_{90} within which 90 % of the probability lie plotted against time for a mass of $m = 10^{10}$ u. Note that the minimum is *not* at zero but at about $r_{90} \approx 0.4 \mu\text{m}$.

using the shorthand notations

$$\beta = -\frac{i\hbar}{8m} \frac{\Delta t}{(\Delta r)^2} \quad \text{and} \quad \gamma = \frac{i\pi G}{\hbar} m^2 \Delta t (\Delta r)^2. \quad (78)$$

We use the tridiagonal matrix algorithm to solve the linear system (71).

4.1 Numerical Results

We start with a spherically symmetric Gaussian wave packet (33) whose width is always set to a value of $a = 0.5 \mu\text{m}$. Note that due to the scaling law (22) the width can be fixed without loss of generality.

The results can be summarised as follows:

- For masses $m \leq 6 \times 10^9$ u the wave packet spreads, but slower than the free solution for zero potential spreads. The larger the mass, the slower the spreading becomes compared to the free solution.

For masses below 10^9 u the difference to the free solution is hardly identifiable.

- For masses $m \geq 7 \times 10^9$ u we observe a collapsing wave packet. The shrinking behaviour was verified for masses up to 3×10^{11} u.
- We have no results for larger masses, yet, as for reliable results one needs to increase both the temporal and spatial resolution with increasing mass, and therefore the runtime of the calculation also increases.

In figure 4 snapshots of a typical collapse are presented. The radial probability density $\rho = 4\pi r^2 |\Psi|^2$ is plotted against r for a mass of $m = 7 \times 10^9$ u.

In figure 5 we plot the time evolution for the global maximum of the probability density. The collapsing behaviour for masses not less than 7×10^9 u is obvious. Also

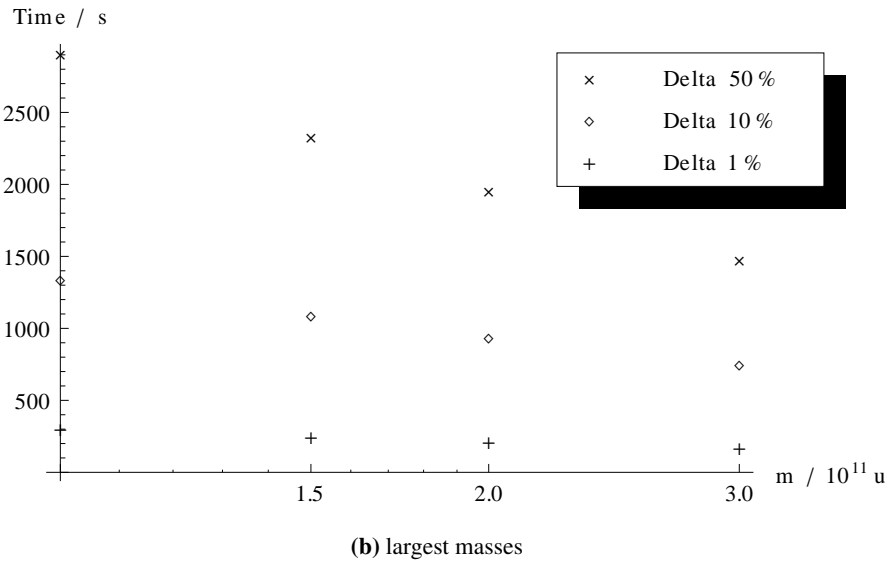
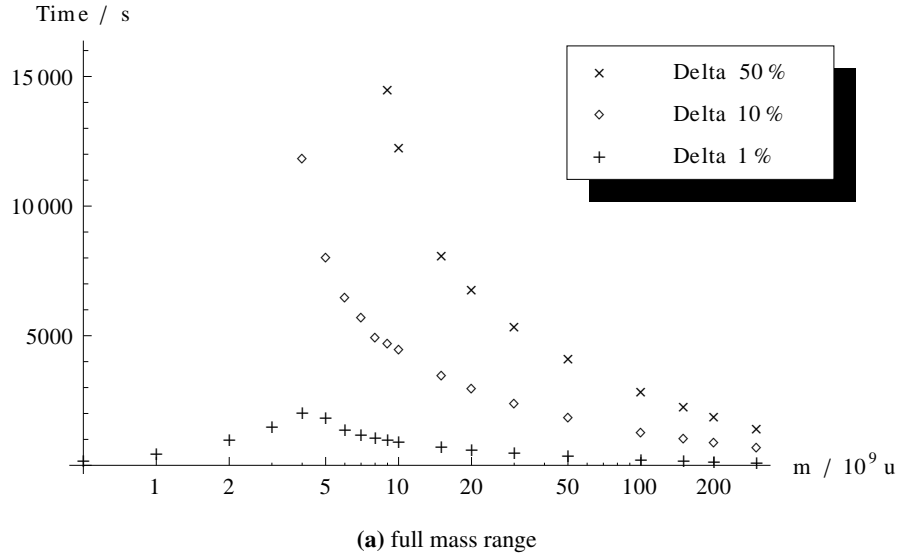


Figure 7: Time it takes until the gravitationally interacting solution differs from the solution of the free Schrödinger equation in its FWHM by a percentage of 1 %, 10 %, and 50 % respectively.

note the oscillations for larger time values which are due to the packet penetrating itself. There also seems to be some equilibrium distance to which the wave packet collapses, which might correspond to a stationary solution. The chaotic behaviour for the curve corresponding to $m = 5 \times 10^{10}$ u is probably due to numeric effects.

We also plot the radius r_{90} within which 90 % of the probability are located, i. e.

$$90 \% = \int_0^{r_{90}} 4\pi r^2 |\Psi|^2 dr, \quad (79)$$

against time. One can see from figure 6, where $r_{90}(t)$ is plotted for a mass of 10^{10} u, that it is reasonable to define a collapse time by the minimum of this plot, which then is about 30 000 seconds.

4.2 Coherence Time

While interferometry experiments might still be feasible at masses of order of the collapse mass of 10^{10} u that we found, another experimental constriction occurs. As can be seen from figures 5 and 6 the time scale beneath which the collapse takes place is of the order of several hours. For experimental tests one would like to take this time scale down to a reasonable value.

Hence, we plot in figure 7 the time it takes the solution of the full SN-equation to differ from the solution of the free Schrödinger equation in its full width at half maximum by a certain percentage against the mass. Figure 7 (a) shows that the coherence time needed decreases with increasing mass. According to figure 7 (b) it takes, for example, about 3 minutes for the solution for $m = 3 \times 10^{11}$ u to differ from the free solution by one per cent.

Consequently on one hand, if keeping the width of the wave packet constant, for an experimental test of the SN-equation by means of e. g. molecular inteferometry one needs to maximise not only the mass but also coherence time and the sensitivity regarding the detection of deviations from the free Schrödinger equation.

But note that on the other hand, we also could make use of the scaling law (22) to decrease the collapse time. If we simultaneously increase the mass by factor of μ and decrease the width by a factor of μ^{-3} the collapse time decreases by a factor of μ^{-5} . Thus, for a mass of 10^{11} u, for example, observed with a grating period of 0.5 nm one should in principle be able to observe a collapsing wave packet causing a loss of interference with a coherence time of approximately 300 ms.

References

- [1] Markus Arndt, Klaus Hornberger, and Anton Zeilinger. Probing the limits of the quantum world. *Physics World*, 18:35–40, 2005.
- [2] Steve Carlip. Is quantum gravity necessary? *Classical and Quantum Gravity*, 25(15):107–144, 2008.
- [3] Domenico Giulini. On Galilei invariance in quantum mechanics and the Bargmann superselection rule. *Annals of Physics (New York)*, 249(1):222–235, 1996.

- [4] Lucia Hackermüller, Stefan Uttenthaler, Klaus Hornberger, Elisabeth Reiger, Björn Brezger, Anton Zeilinger, and Markus Arndt. Wave nature of biomolecules and fluorofullerenes. *Physical Review Letters*, 91(9):090408 (4 pages), 2003.
- [5] Richard Harrison, Irene Moroz, and Paul Tod. A numerical study of the Schrödinger-Newton equations. *Nonlinearity*, 16:101–122, 2003.
- [6] Elliott H. Lieb. Existence and uniqueness of the minimizing solutions of Choquard’s nonlinear equation. *Studies in Applied Mathematics*, 57:93–105, 1977.
- [7] Irene Moroz, Roger Penrose, and Paul Tod. Spherically-symmetric solutions to the Schrödinger-Newton equations. *Classical and Quantum Gravity*, 15(9):2733–2742, 1998.
- [8] Remo Ruffini and Silvano Bonazzola. Systems of self-gravitating particles in General Relativity and the concept of an equation of state. *Physical Review*, 187(5):1767–1783, 1969.
- [9] Peter Jay Salzman and Steve Carlip. A possible experimental test of quantized gravity. arXiv:gr-qc/0606120. Based on the Ph.D. thesis of P. Salzman: “Investigation of the Time Dependent Schrödinger-Newton Equation”, Univ. of California at Davis, 2005.